GEOPHYSICS, VOL. 82, NO. 6 (NOVEMBER-DECEMBER 2017); P. C229–C240, 16 FIGS., 2 TABLES.
10.1190/GEO2017-0215.1

A new parameterization for acoustic orthorhombic media

Shibo Xu[1] and Alexey Stovas[1]

ABSTRACT

We have defined a group of new parameterizations for P-wave in acoustic orthorhombic (ORT) media with three cross-term normal moveout velocities and three cross-term anellipticity parameters. The corresponding perturbation-based approximations for traveltime in ORT model are developed using the new parameterizations. The perturbation coefficients are computed by solving the eikonal equation in corresponding parameterization. Eight types of parameterization are defined based on the different elliptical background model and selection of anellipticity parameters. As the traveltime can be converted from the group velocity inverse, the sensitivity of the group velocity inverse to anellipticity parameters is analyzed for different parameterizations and different range of offsets. To stabilize the perturbation series and improve the accuracy, the Shanks transform is applied. From the comparison of traveltime after the Shanks transform using different parameterizations, we have concluded that the parameterization with vertical, two horizontal velocities, and three cross-term anellipticity parameters results in the best accuracy of traveltime function for P-wave in acoustic ORT medium.

INTRODUCTION

Traveltime approximations are commonly used in seismic data processing such as velocity analysis, modeling, and time migration (Červený, 2001; Yilmaz, 2001). The estimation for model parameters in velocity analysis depends on the accuracy of the traveltime approximation. For time domain migration, the accuracy of the result is also dependent on the traveltime approximation used in modeling part. In homogeneous isotropic or elliptical isotropic media, the moveout function has a hyperbolic form. We need to take nonhyperbolicity (driven by anellipticity parameters) into consideration because it commonly exists and plays an important role in seismic data processing and interpretation, especially for large offsets. The moveout function has a nonhyperbolic form in anisotropic media. Nonhyperbolic (long-spread) moveout is often used in the velocity analysis of P-waves in transversely isotropic media with a vertical symmetry axis (VTI). The P-wave time domain signature in a VTI model depends on two interval parameters: normal moveout (NMO) velocity from a horizontal reflector and the anellipticity coefficient η (Alkhalifah and Tsvankin, 1995; Tsvankin, 2005). Different nonhyperbolic moveout approximations for a homogeneous VTI are listed and discussed by Fowler (2003), Fomel (2004), and Golikov and Stovas (2012). Fomel and Stovas (2010) derive a generalized nonhyperbolic moveout approximation for the traveltime approximation defined from zero-offset and one nonzero-offset ray computation. Alkhalifah (2011) proposes the traveltime expression with series in terms of anelliptic parameter η by solving the eikonal equation for acoustic VTI medium and by applying the Shanks transform to obtain higher accuracy.

The orthorhombic (ORT) model is introduced by Schoenberg and Helbig (1997) to describe fractured reservoirs, and it well explains the azimuthal dependency in surface seismic data. Tsvankin (1997, 2012) defines nine elastic model parameters for an ORT model that can be reduced to six parameters in an acoustic approximation (Alkhalifah, 2003). The first-order curvatures are defined by the NMO velocity ellipse (Grechka and Tsvankin, 1999a, 1999b), and the second-order curvatures are defined by the azimuth-dependent anellipticity. Vasconcelos and Tsvankin (2006) derive the nonhyperbolic moveout of P-wave in ORT media using the NMO velocities V_{n1} and V_{n2} defined in vertical symmetry planes, and the anellipticity parameters η_1, η_2, and η_3 defined in all three symmetry planes. Note that η_1 and η_2 are the anellipticity parameters defined in $[XOZ]$ and $[YOZ]$ symmetry planes and η_3 is the anellipticity parameter defined in $[XOY]$ plane (Vasconcelos and Tsvankin, 2006). Stovas (2015) derives the azimuthally dependent kinematic properties of the ORT media and introduces new anellipticity parameter η_{xy}. Sripanich and Fomel (2015) modify the anelliptic functional form of Fomel (2004) and extend it to ORT model to approximate P-wave phase and

Manuscript received by the Editor 10 April 2017; revised manuscript received 8 July 2017; published ahead of production 23 August 2017; published online 05 October 2017.
[1]Norwegian University of Science and Technology, Department of Geoscience and Petroleum, Trondheim, Norway. E-mail: shibo.xu@ntnu.no; alexey.stovas@ntnu.no.

group velocities. Alkhalifah (2013) and Masmoudi and Alkhalifah (2014) develop this concept to approximate traveltime in horizontal transversely isotropic media with arbitrary symmetry-axis azimuth ϕ and estimate the anisotropy parameter η and the azimuthal angle ϕ. The perturbation-based moveout approximation with a traditional elliptic background for ORT media is discussed by Stovas et al. (2016). The traveltime approximation for the ORT model using perturbation theory by other anellipticity parameters in an inhomogeneous background medium is developed by Masmoudi and Alkhalifah (2016). Xu et al. (2017) propose a new set of moveout approximations based on the perturbation series in anellipticity parameter using the alternative elliptical background model defined by the vertical and horizontal velocities in a homogeneous ORT media. A horizontally layered ORT medium with parameters computed for the fourth-order moveout is studied in Koren and Ravve (2017) and Ravve and Koren (2017). Different parameterization impacts the accuracy of the traveltime approximation due to different proportion in perturbation parameters (anellipticity parameters) and the anisotropy estimation in velocity analysis depends on the accuracy of the traveltime approximation. The subsurface parameterization also plays an important role in sensitivity and trade-off analysis for full-waveform inversion in acoustic anisotropic medium (Alkhalifah and Plessix, 2014; Gholami et al., 2013).

In this paper, we define new parameterizations for acoustic ORT medium with different combinations of elliptical background and anellipticity coefficients. The list of parameterization including eight different ones is split into symmetric and nonsymmetric groups. The sensitivity analysis to anellipticity parameters at near, mid, and far offset is performed for the group velocity inverse. The parameterization with vertical and two horizontal velocities and three cross-term anellipticity parameters results in the most accurate approximation based on the Shanks transform as it shown in the numerical example.

A NEW PARAMETERIZATION FOR AN ACOUSTIC ORT MODEL

The symmetry behavior of the ORT model is commonly used to describe the fractured formation. ORT media have three mutually orthogonal symmetry planes: two vertical and one horizontal. Six model parameters are defined for acoustic ORT model (Alkhalifah, 2003). Vasconcelos and Tsvankin (2006) represent the ORT model by the vertical velocity V_0, two NMO velocities V_{n1} and V_{n2} defined in corresponding $[XOZ]$ and $[YOZ]$ symmetry planes, and three anellipticity parameters η_1, η_2, and η_3 defined in $[XOZ]$, $[YOZ]$, and $[XOY]$ symmetry planes, respectively. Stovas (2015) develops azimuthally dependent properties of the acoustic ORT model using the parameters V_0, V_{n1}, V_{n2}, η_1, η_2, and η_{xy}.

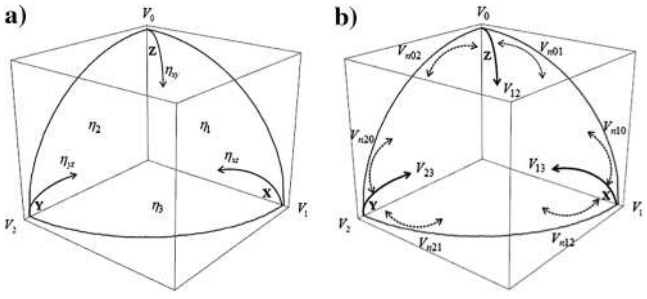

Figure 1. Sketch for cross-term anellipticity parameters: (a) η_{xy}, η_{xz}, and η_{yz} and cross-term NMO velocities: (b) V_{12}, V_{13}, and V_{23} in the ORT model.

In this paper, we define three cross-term anellipticity parameters η_{xy}, η_{xz}, and η_{yz} (Figure 1a) by

$$\eta_{xy} = \sqrt{\frac{(1+2\eta_1)(1+2\eta_2)}{(1+2\eta_3)}} - 1,$$
$$\eta_{xz} = \sqrt{\frac{(1+2\eta_1)(1+2\eta_3)}{(1+2\eta_2)}} - 1,$$
$$\eta_{yz} = \sqrt{\frac{(1+2\eta_2)(1+2\eta_3)}{(1+2\eta_1)}} - 1. \tag{1}$$

Note that the cross-term η_{xy} is defined by Stovas (2015). Each cross-term anellipticity parameter is represented by all three anellipticity parameters (η_1, η_2, and η_3) from corresponding symmetry plane. The inverse transformations of anellipticity parameters are given by

$$\eta_1 = \frac{(1+\eta_{xy})(1+\eta_{xz})-1}{2},$$
$$\eta_2 = \frac{(1+\eta_{xy})(1+\eta_{yz})-1}{2},$$
$$\eta_3 = \frac{(1+\eta_{xz})(1+\eta_{yz})-1}{2}. \tag{2}$$

The NMO velocities in the ORT model (Figure 1b) are defined by the curvatures in corresponding symmetry planes

$$V^2_{n01} = \frac{V^2_{h1}}{1+2\eta_1}, \quad V^2_{n02} = \frac{V^2_{h2}}{1+2\eta_2}, \quad V^2_{n10} = \frac{V^2_0}{1+2\eta_1},$$
$$V^2_{n12} = \frac{V^2_{h2}}{1+2\eta_3}, \quad V^2_{n20} = \frac{V^2_0}{1+2\eta_2}, \quad V^2_{n21} = \frac{V^2_{h1}}{1+2\eta_3}. \tag{3}$$

Note that here $V_{n01} = V_{n1}$ and $V_{n02} = V_{n2}$. We define new NMO velocities by the geometric averaging of corresponding NMO velocities from equation 3,

$$V^2_{12} = V_{n01}V_{n02} = \frac{V_{h1}V_{h2}}{\sqrt{(1+2\eta_1)(1+2\eta_2)}},$$
$$V^2_{13} = V_{n10}V_{n12} = \frac{V_0 V_{h2}}{\sqrt{(1+2\eta_1)(1+2\eta_3)}},$$
$$V^2_{23} = V_{n20}V_{n21} = \frac{V_0 V_{h1}}{\sqrt{(1+2\eta_2)(1+2\eta_3)}}. \tag{4}$$

The definition of the indices is slightly different for NMO velocities. For the NMO velocities V_{nij}, i and j are corresponding to the axis because we use V_0 for the vertical velocity, V_1 and V_2 for the two horizontal velocities, respectively. The indices for cross-term NMO velocity V_{ij} are defined corresponding to the symmetry plane, where 1,2, and 3 represent $[XOZ]$, $[YOZ]$, and $[XOY]$ symmetry planes, respectively.

The inverse transformations for the vertical velocity V_0 and horizontal velocities V_{h1} and V_{h2} are given by

$$V_0^2 = \frac{V_{13}^2 V_{23}^2}{V_{12}^2}(1+2\eta_3) = \frac{V_{13}^2 V_{23}^2}{V_{12}^2}(1+\eta_{xz})(1+\eta_{yz}),$$
$$V_{h1}^2 = \frac{V_{12}^2 V_{23}^2}{V_{13}^2}(1+2\eta_2) = \frac{V_{12}^2 V_{23}^2}{V_{13}^2}(1+\eta_{xy})(1+\eta_{yz}),$$
$$V_{h2}^2 = \frac{V_{12}^2 V_{13}^2}{V_{23}^2}(1+2\eta_1) = \frac{V_{12}^2 V_{13}^2}{V_{23}^2}(1+\eta_{xy})(1+\eta_{xz}). \quad (5)$$

Eight types of parameterization for acoustic ORT model based on different elliptical background model and anellipticity parameters are listed in Table 1. Based on the symmetric behavior, these parameterizations are divided into two groups: nonsymmetrical (cases A–D) and symmetrical (cases E–H). We illustrate two groups of parameterization in Figures 2 and 3, respectively. To perform the sensitivity analysis, we select the parameterization with V_0, V_{h1}, V_{h2}, η_{xy}, η_{xz}, and η_{yz} (case H) as an example for the following analysis.

Table 1. Eight types of parameterizations with different background model and different set of anellipticity parameters.

Parameterization	Elliptical background	Anellipticity parameters
	Nonsymmetric parameterizations	
Case A	V_0, V_{n1}, V_{n2}	η_1, η_2, η_3
Case B	V_0, V_{n1}, V_{n2}	$\eta_1, \eta_2, \eta_{xy}$
Case C	V_0, V_{n1}, V_{n2}	$\eta_{xy}, \eta_{xz}, \eta_{yz}$
Case D	V_0, V_{h1}, V_{h2}	$\eta_1, \eta_2, \eta_{xy}$
	Symmetric parameterizations	
Case E	V_{12}, V_{13}, V_{23}	η_1, η_2, η_3
Case F	V_{12}, V_{13}, V_{23}	$\eta_{xy}, \eta_{xz}, \eta_{yz}$
Case G	V_0, V_{h1}, V_{h2}	η_1, η_2, η_3
Case H	V_0, V_{h1}, V_{h2}	$\eta_{xy}, \eta_{xz}, \eta_{yz}$

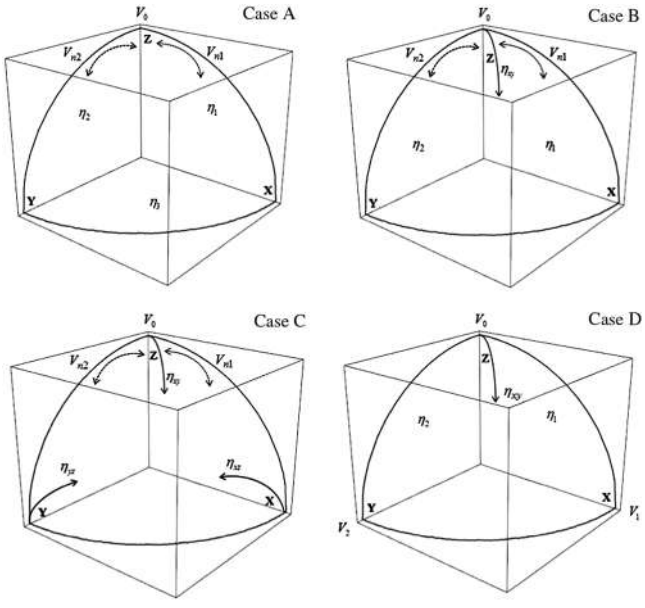

Figure 2. Sketch for nonsymmetric parameterizations for the acoustic ORT model defined by cases A–D.

PERTURBATION-BASED TRAVELTIME APPROXIMATION USING A NEW PARAMETERIZATION

The perturbation series for traveltime (Stovas et al., 2016) in terms of new cross-term anellipticity parameters is defined up to the second order by

$$\tau = \tau_0 + \sum_i a_i \eta_i + \sum_{i,j} b_{ij} \eta_i \eta_j, \quad (i,j = 1,2,3), \quad (6)$$

where the index $1 \equiv xy$, $2 \equiv xz$, and $3 \equiv yz$. The elliptical background model is given by

$$\tau_0 = \sqrt{t_0^2 + \frac{x^2}{V_{h1}^2} + \frac{y^2}{V_{h2}^2}}, \quad (7)$$

where t_0 is the vertical traveltime with $t_0 = z/V_0$.

The ORT eikonal equation (Alkhalifah, 2003) with the new parameterization takes the form

$$V_0^2\left(\frac{\partial\tau}{\partial z}\right)^2 + V_{h1}^2\left(\frac{\partial\tau}{\partial x}\right)^2 + V_{h2}^2\left(\frac{\partial\tau}{\partial y}\right)^2$$
$$- \left(\frac{(1+\eta_{xy})(1+\eta_{xz})-1}{(1+\eta_{xy})(1+\eta_{xz})}\right) V_{h1}^2 V_0^2 \left(\frac{\partial\tau}{\partial x}\right)^2 \left(\frac{\partial\tau}{\partial z}\right)^2$$
$$- \left(\frac{(1+\eta_{xy})(1+\eta_{yz})-1}{(1+\eta_{xy})(1+\eta_{yz})}\right) V_{h2}^2 V_0^2 \left(\frac{\partial\tau}{\partial y}\right)^2 \left(\frac{\partial\tau}{\partial z}\right)^2$$
$$- \left(\frac{(1+\eta_{xz})(1+\eta_{yz})-1}{(1+\eta_{xz})(1+\eta_{yz})}\right) V_{h1}^2 V_{h2}^2 \left(\frac{\partial\tau}{\partial x}\right)^2 \left(\frac{\partial\tau}{\partial y}\right)^2$$
$$+ \left(\frac{\eta_{xz}\eta_{yz} + \eta_{xy}((1+\eta_{xz})(1+\eta_{yz})-1)}{(1+\eta_{xy})(1+\eta_{xz})(1+\eta_{yz})}\right) V_{h1}^2 V_{h2}^2 V_0^2$$
$$\times \left(\frac{\partial\tau}{\partial x}\right)^2 \left(\frac{\partial\tau}{\partial y}\right)^2 \left(\frac{\partial\tau}{\partial z}\right)^2 = 1. \quad (8)$$

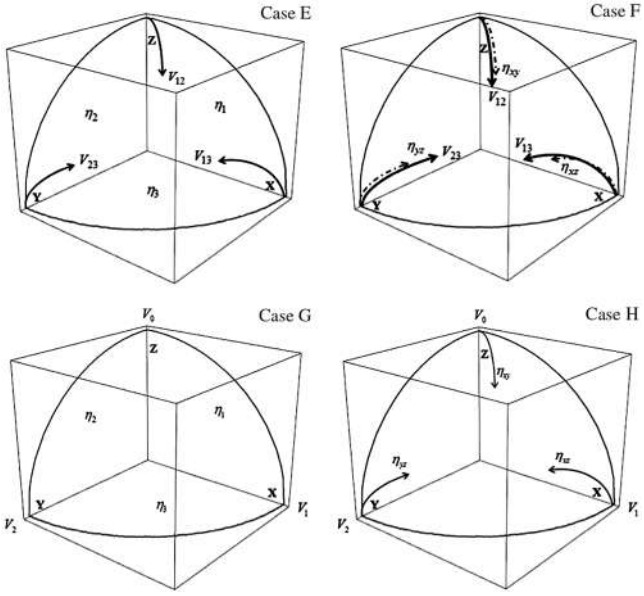

Figure 3. Sketch for symmetric parameterizations for the acoustic ORT model defined by cases E–H.

Solving the eikonal equation 8 with the corresponding perturbation series in equation 6, we obtain the series coefficients a_i and b_{ij} $(i, j = 1, 2, 3)$ that are given in Appendix A.

To obtain greater accuracy, the Shanks transform (Bender and Orszag, 1978) is applied by the form

$$\tau_3 = \tau_0 + \frac{\tau_1^2}{\tau_1 - \tau_2}, \tag{9}$$

where τ_0 is defined in equation 7, $\tau_1 = \sum_i a_i \eta_i$ and $\tau_2 = \sum_{ij} b_{ij} \eta_i \eta_j$ are the first- and second- order terms in equation 6.

To test the sensitivity of the perturbation coefficients a_i and b_{ij}, we select the ORT model with the parameters: $V_0 = 2$ km/s, $V_{h1} = 2.4$ km/s, $V_{h2} = 2.6$ km/s, $\eta_1 = 0.15$, $\eta_2 = 0.18$, and $\eta_3 = 0.1$. The perturbation coefficients a_i and b_{ij} $(i, j = 1, 2, 3)$ from our proposed parameterization (V_0, V_{h1}, V_{h2}, η_{xy}, η_{xz}, and η_{yz}, case H) are plotted in Figures 4, 5, and 6, respectively. One can see that the shape of the first-order coefficients a_2 and a_3 is very similar and the magnitude of them is larger than the coefficient a_1. For quadratic coefficients, similarly, the coefficients b_{22} and b_{33} are larger than b_{11} in magnitude. Note that the magnitude of the first- and second-order coefficients a_1 and b_{11} is changing dramatically at near offsets. The magnitude of three cross-term coefficients is quite similar, whereas the shape of cross-term b_{23} is very complicated.

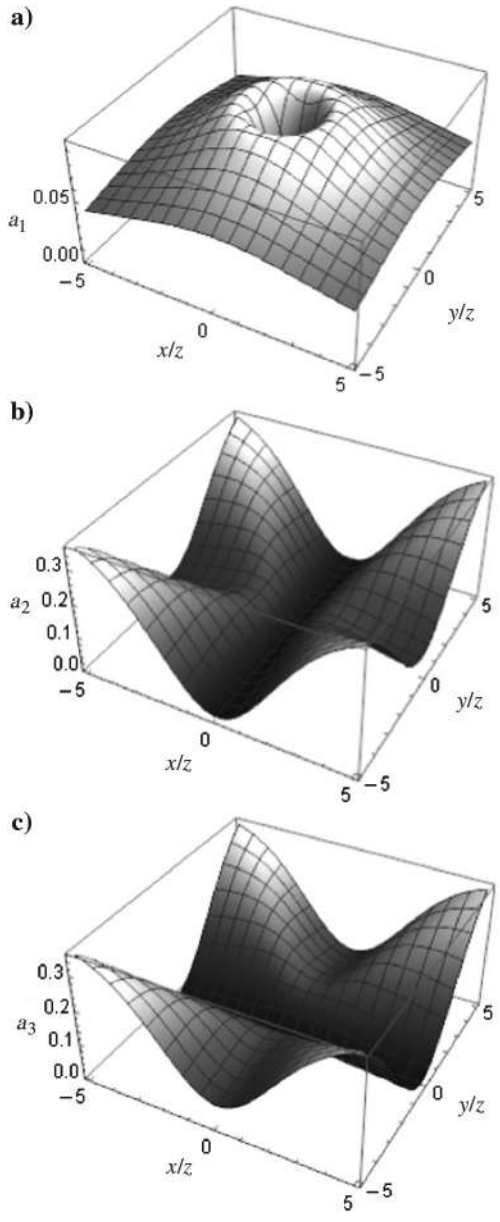

Figure 4. The first-order perturbation coefficients a_i (case H). Coefficients a_1, a_2, and a_3 are shown in panels (a-c), respectively.

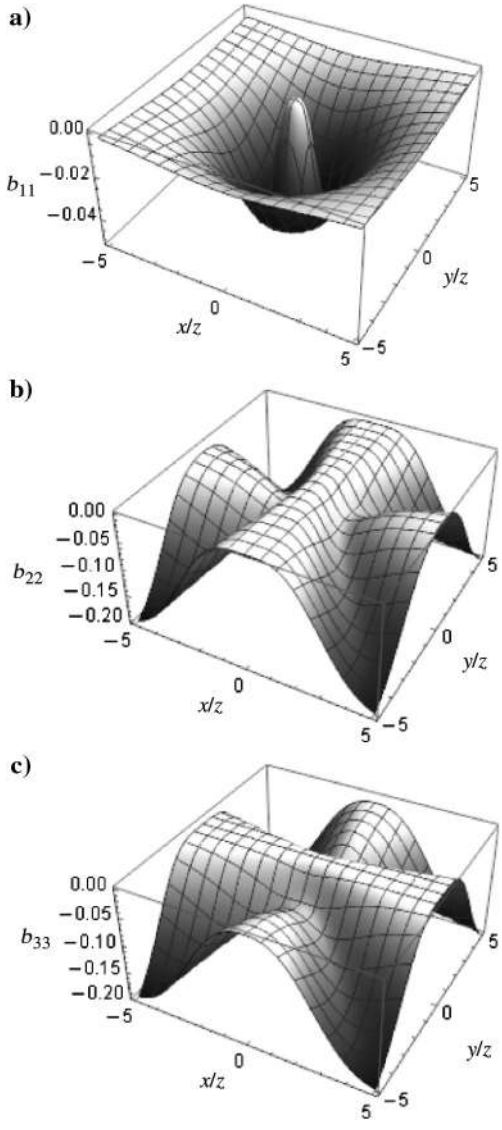

Figure 5. The quadratic perturbation coefficients b_{ii} (case H). Coefficients b_{11}, b_{22}, and b_{33} are shown in panels (a-c), respectively.

THE SENSITIVITY OF TRAVELTIME TO ANELLIPTICITY PARAMETERS

To analyze the sensitivity of traveltime to anellipticity parameters, we define the group velocity inverse related coefficients $\tilde{a}_i$ and $\tilde{b}_{ij}$ by

$$\frac{1}{V(\theta,\phi)} = \frac{1}{\tilde{V}_0(\theta,\phi)} + \sum_i \tilde{a}_i(\theta,\phi)\eta_i + \sum_{i,j} \tilde{b}_{ij}(\theta,\phi)\eta_i\eta_j, \tag{10}$$

where

$$\frac{1}{\tilde{V}_0(\theta,\phi)} = \frac{\tau_0 \cos\theta}{z}(x = z\tan\theta\cos\phi,\ y = z\tan\theta\sin\phi),$$
$$\tilde{a}_i(\theta,\phi) = \frac{a_i\cos\theta}{z}(x = z\tan\theta\cos\phi,\ y = z\tan\theta\sin\phi),$$
$$\tilde{b}_{ij}(\theta,\phi) = \frac{b_{ij}\cos\theta}{z}(x = z\tan\theta\cos\phi,\ y = z\tan\theta\sin\phi), \tag{11}$$

where τ_0 is defined in equation 7, coefficients a_i and b_{ij} are given in Appendix A, θ is the dip angle to the vertical, and the azimuth ϕ is the azimuth defined from the x-axis. To analyze the sensitivity at differ-

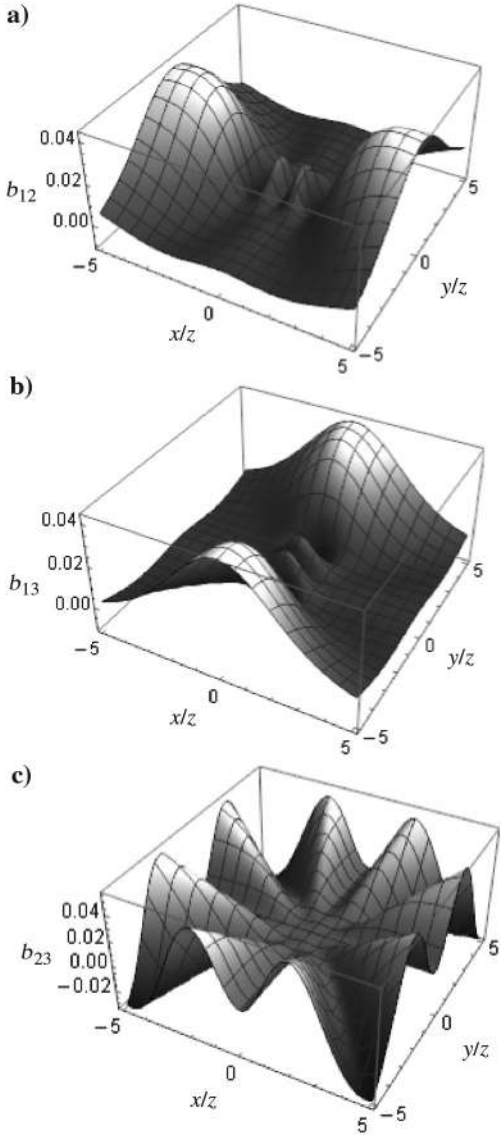

Figure 6. The cross-term perturbation coefficients b_{ij}, $(i \neq j)$ (case H). Coefficients b_{12}, b_{13}, and b_{23} are shown in panels (a-c), respectively.

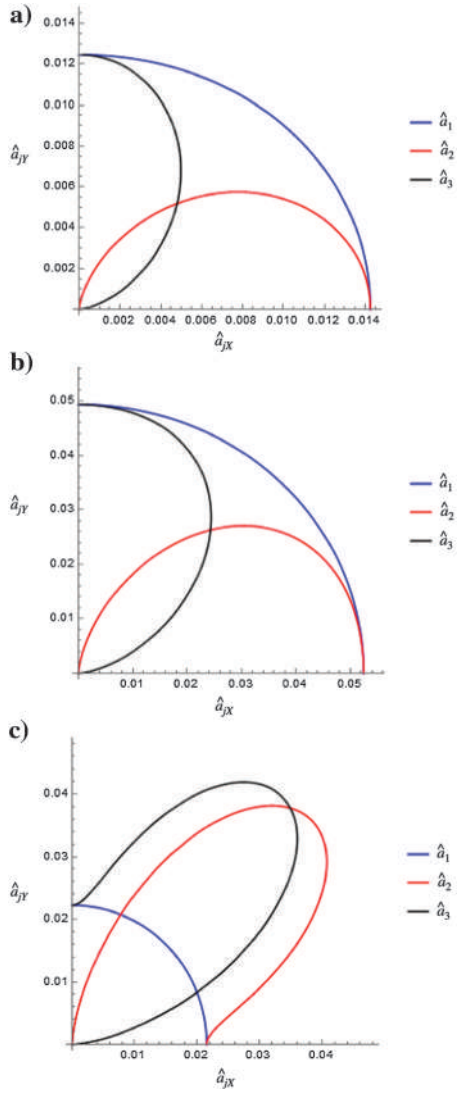

Figure 7. The first-order sensitivity coefficients $\hat{a}_i$ in case H for (a) short offset ($\theta \in (0^\circ, 30^\circ)$), (b) intermediate offset ($\theta \in (30^\circ, 60^\circ)$), and (c) far offset ($\theta \in (60^\circ, 90^\circ)$). The coefficients a_1, a_2, and a_3 are shown by the blue, red, and black colors, respectively.

ent offset range, we compute the integral from coefficients $\tilde{a}_i$ and $\tilde{b}_{ij}$ with respect to different range of dip angle θ ($\theta \in (0^\circ, 30^\circ)$, (30°, 60°) and (60°, 90°)) that corresponding to near, mid, and far offset,

$$\hat{a}_i(\phi) = \frac{1}{\theta_2 - \theta_1}\int_{\theta_1}^{\theta_2} \tilde{a}_i(\theta,\phi)d\theta,$$
$$\hat{b}_{ij}(\phi) = \frac{1}{\theta_2 - \theta_1}\int_{\theta_1}^{\theta_2} \tilde{b}_{ij}(\theta,\phi)d\theta. \quad (12)$$

The polar plots for the sensitivity coefficients $\hat{a}_i$ and $\hat{b}_{ij}$ versus azimuth ϕ for model with parameterization (case H) for the near, mid, and far offset are shown in Figures 7a–7c, 8a–8c, and 9a–9c, respectively. One can see that the first- and quadratic-order coefficients have similar sensitivity plots. The sensitivity in anellipticity parameter η_{xy} has an elliptic shape in the $[XOY]$ plane regardless of the range of offsets. The sensitivities to anellipticity parameters η_{xz} and η_{yz} reach the maximum values for 0 and $\pi/2$ azimuth angle, respectively. This is valid for the near and mid offset. The reason is that the impact of anellipticity parameter η_3 is not dominating for the near- and mid-offset range. For a large offset, the effect of η_3 starts to dominate in $\hat{a}_2$ and $\hat{a}_3$ resulting in pronounced anomaly at approximately 45° azimuth angle. The azimuthal behavior of the cross-term coefficients b_{ij}, $(i \neq j)$ is more complicated (Figure 9). One can see that coefficients $\hat{b}_{12}$ and $\hat{b}_{13}$ are symmetric, whereas the magnitude of $\hat{b}_{23}$ increases with an increase in offset. There is almost no impact from $\hat{b}_{23}$ ($\eta_{xz}\eta_{yz}$) at a near offset because the crosstalk between η_{xz} and η_{yz} is very small. With an increase in offset, the crosstalk becomes more pronounced and the magnitude of coefficient $\hat{b}_{23}$ increases at a far offset. The cross-term coefficients $\hat{b}_{12}$ ($\eta_{xy}\eta_{xz}$) and $\hat{b}_{13}$ ($\eta_{xy}\eta_{yz}$) become equal at approximately 45° azimuth at any offset range while mostly being focused along the x- and y-axes, respectively.

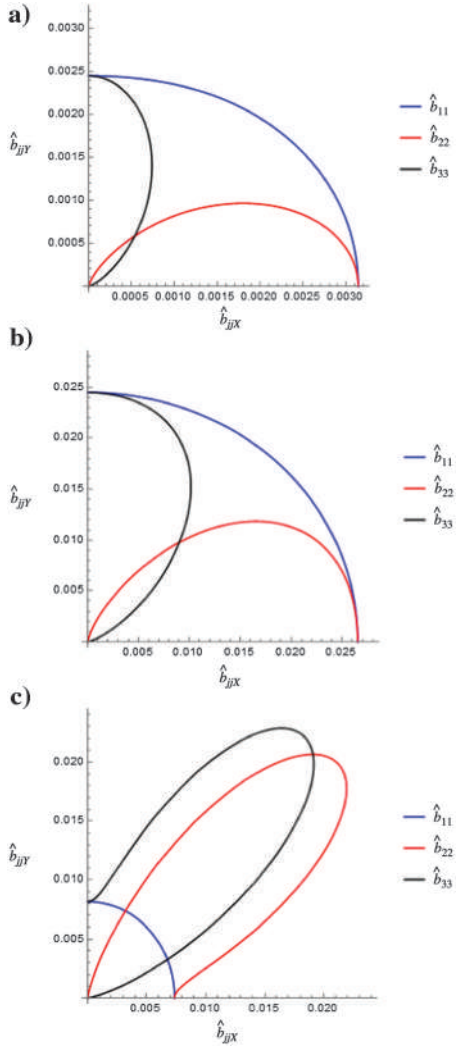

Figure 8. The quadratic sensitivity coefficients $\hat{b}_{ii}$ in case H for (a) short offset ($\theta \in (0^\circ, 30^\circ)$), (b) intermediate offset ($\theta \in (30^\circ, 60^\circ)$), and (c) far offset ($\theta \in (60^\circ, 90^\circ)$). The coefficients b_{11}, b_{22}, and b_{33} are shown by the blue, red, and black colors, respectively.

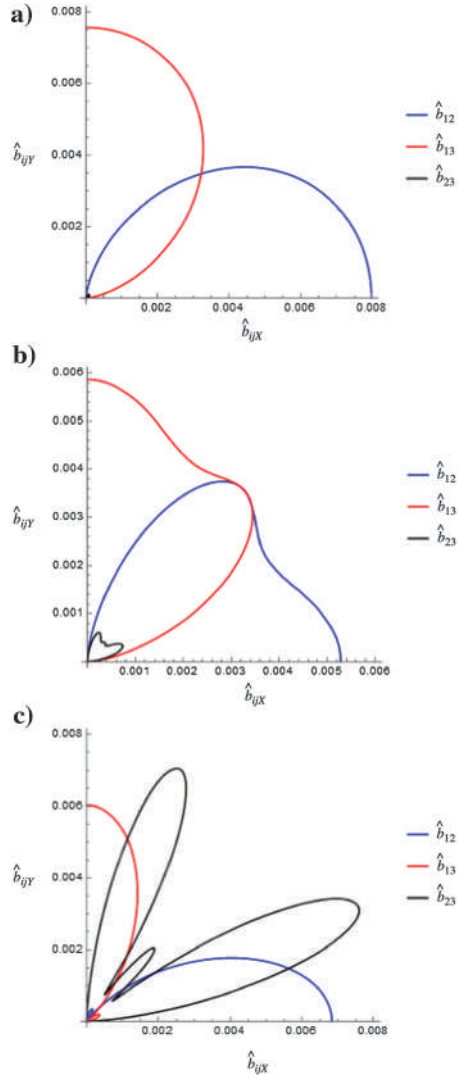

Figure 9. The cross-term sensitivity coefficients b_{ij}, $(i \neq j)$ in case H for (a) short offset ($\theta \in (0^\circ, 30^\circ)$), (b) intermediate offset ($\theta \in (30^\circ, 60^\circ)$), and (c) far offset ($\theta \in (60^\circ, 90^\circ)$). The coefficients b_{12}, b_{13}, and b_{23} are shown by the blue, red, and black colors, respectively.

The overall sensitivity coefficients $\hat{A}_i$ and $\hat{B}_{ij}$ can be computed in a similar way as the ones given in equations 12 but with double integrals over the entire angle range,

$$\hat{A}_i = \frac{4}{\pi^2}\int_0^{\pi/2}\int_0^{\pi/2} \tilde{a}_i(\theta,\phi)d\theta d\phi,$$
$$\hat{B}_{ij} = \frac{4}{\pi^2}\int_0^{\pi/2}\int_0^{\pi/2} \tilde{b}_{ij}(\theta,\phi)d\theta d\phi. \quad (13)$$

The overall sensitivities are illustrated in Figure 10. One can see that $\hat{A}_1 > \hat{A}_2 > \hat{A}_3$ and $\hat{B}_{11} > \hat{B}_{22} > \hat{B}_{33}$. The inequalities for the first-order $\hat{A}_i$ and quadratic $\hat{B}_{ii}$ coefficients are controlled by the semi-axes for elliptical background model. For this parameterization (case H), we have $1/V_0^2 > 1/V_{h1}^2 > 1/V_{h2}^2$, and this inequality explains the behavior of sensitivity coefficients. A similar analysis can be performed for other background models used in our tests.

To see the difference in the overall sensitivities between different parameterizations, Figures 11 and 12 show the second-order coefficients $\hat{B}_{ij}$ computed from all parameterizations listed in Table 1. One can see that the tendency is $\hat{B}_{11} > \hat{B}_{22} > \hat{B}_{33}$ for all the cases except for cases E and F. This behavior can also be explained by the corresponding slownesses, $1/V_{23}^2 > 1/V_{13}^2 > 1/V_{12}^2$. Note that the magnitude of $\hat{B}_{ij}$ computed for parameterization case H is the smallest among all parameterizations. Note that we use the term group velocity inverse ($1/V_{\text{group}}$) instead of traveltime for the sensitivity analysis because the traveltime can be converted from it and because there is no asymptotic behavior for traveltime at infinite offset, taking the integral along the offset up to infinite for traveltime is impossible to get the overall sensitivity in anellipticity parameters.

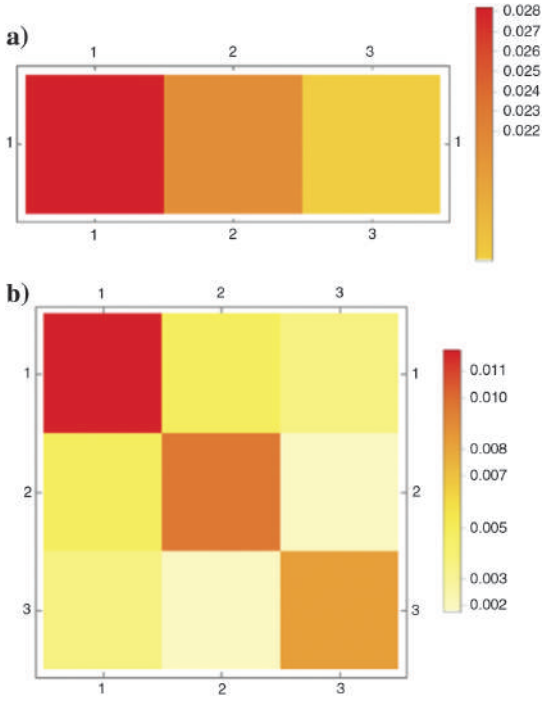

Figure 10. The overall sensitivity coefficients: (a) first order and (b) second order using parameterization case H. The coefficients $\hat{A}_1$, $\hat{A}_2$, and $\hat{A}_3$ are shown from left to right. The second-order coefficients are composed in matrix form with indices $1 \equiv \eta_{xy}$, $2 \equiv \eta_{xz}$, and $3 \equiv \eta_{yz}$.

NUMERICAL EXAMPLES

Using the ORT model from Table 2, the relative error in traveltime using the parameterization case H computed from perturbation series in equation 6 and the Shanks transform in equation 9 are shown in

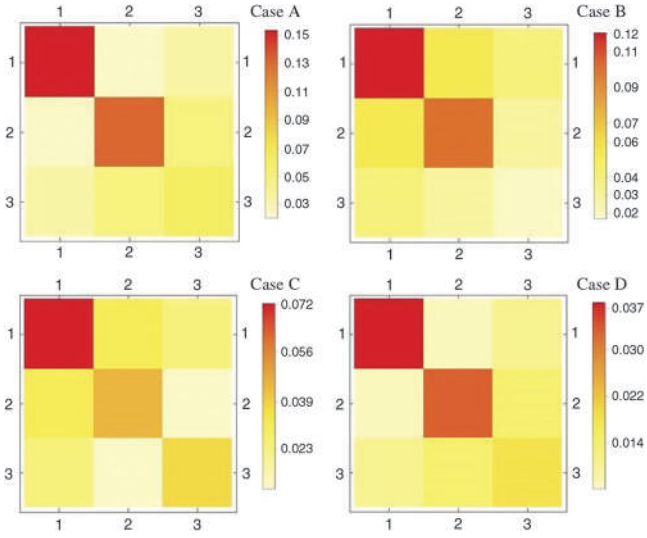

Figure 11. The second-order overall sensitivity coefficients $\hat{B}_{ij}$ using nonsymmetric parameterizations cases A–D. The second-order coefficients are composed in matrix form with indices $1 \equiv \eta_1$, $2 \equiv \eta_2$, and $3 \equiv \eta_3$ for case A, $1 \equiv \eta_1$, $2 \equiv \eta_2$, and $3 \equiv \eta_{xy}$ for cases B and D, and $1 \equiv \eta_{xy}$, $2 \equiv \eta_{xz}$, and $3 \equiv \eta_{yz}$ for case C.

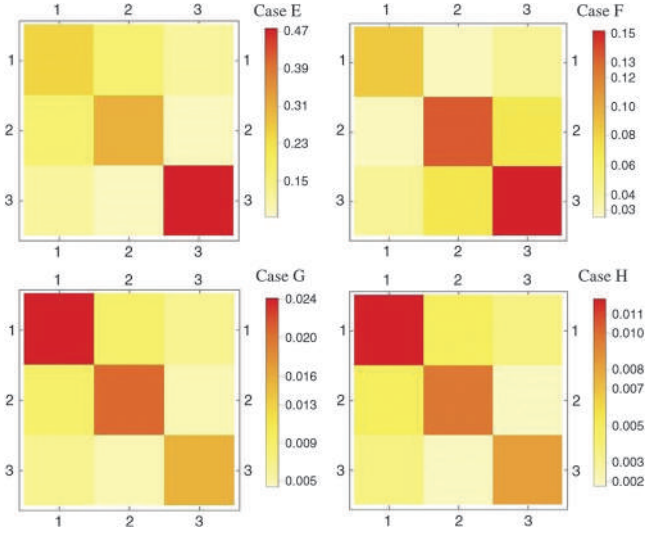

Figure 12. The second-order overall sensitivity coefficients $\hat{B}_{ij}$ using symmetric parameterizations cases E–H. The second-order coefficients are composed in matrix form with indices $1 \equiv \eta_1$, $2 \equiv \eta_2$, and $3 \equiv \eta_3$ for cases E and G and $1 \equiv \eta_{xy}$, $2 \equiv \eta_{xz}$, and $3 \equiv \eta_{yz}$ for cases F and H.

Table 2. The ORT model parameters.

Velocities (km/s)	V_0	V_{h1}	V_{h2}	V_{n1}	V_{n2}	V_{12}	V_{13}	V_{23}
	2	2.4	2.6	2.1	2.23	2.17	2.04	1.94
Anellipticity parameters	η_1	η_2	η_3	η_{xy}	η_{xz}	η_{yz}		
	0.15	0.18	0.1	0.214	0.07	0.12		

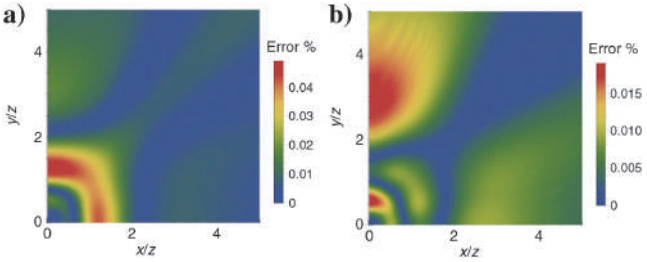

Figure 13. The relative error of (a) perturbation series and (b) the Shanks transform for traveltime with parameterization case H.

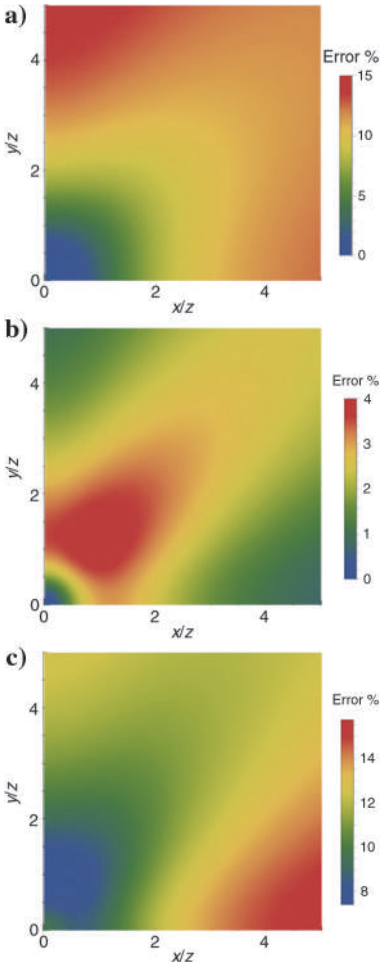

Figure 14. The relative error in traveltime using the hyperboloid approximation with (a) vertical and two NMO velocities, (b) vertical and two horizontal velocities, and (c) three cross-term NMO velocities.

Figure 13a and 13b, respectively. One can see that the Shanks transform significantly improves the accuracy of the approximation.

Our set of parameterizations is based on three types of background models and three types of anellipticity coefficients. To compare the accuracy of the Shanks transform using different parameterizations from Table 1 and analyze their impact, the relative error in traveltime using three different elliptical background models — (V_0, V_{n1}, V_{n2}), (V_0, V_{h1}, V_{h2}), and (V_{12}, V_{13}, V_{23}) — is shown in Figure 14. One can see that the elliptical background model using vertical and two horizontal velocities is the most accurate one, whereas the one using the cross-term NMO velocities results in the worst accuracy even for a short offset.

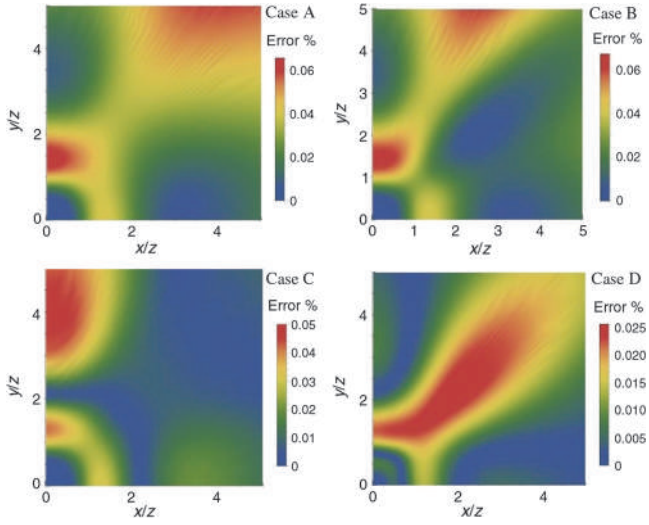

Figure 15. The relative error in traveltime of the Shanks transform for parameterizations from cases A–D.

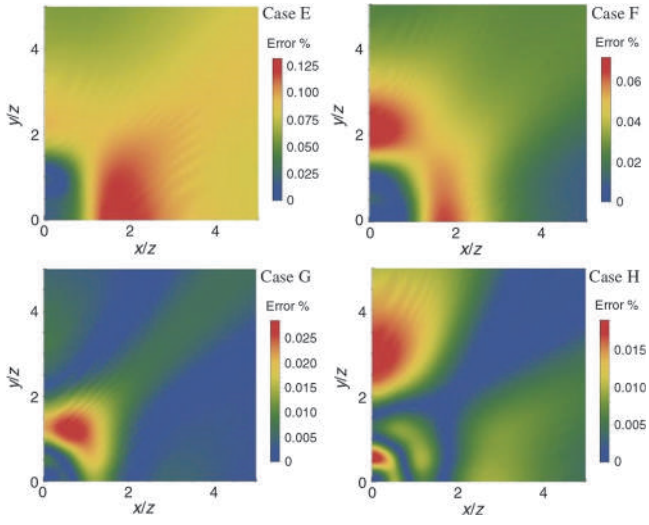

Figure 16. The relative error in traveltime of the Shanks transform for parameterizations from cases E–H.

The relative error in traveltime from the Shanks transform in equation 9 using the ORT model (Table 2) for all nonsymmetric and symmetric parameterizations (Table 1) is shown in Figures 15 and 16, respectively. Note that all the accuracy plots are computed from the same ORT model but using different parameterizations. For parameterization cases A, B, D, and G, the perturbation series coefficients for traveltime approximation are discussed by Xu et al. (2017). The perturbation series coefficients a_i and b_{ij} for cases C, E, and F are given in Appendices B, C, and D, respectively. From a comparison of plots in Figures 15 and 16, one can see that the accuracy is mostly driven by the selection of background model. The parameterization with the vertical and two horizontal velocities is generally more accurate, whereas the parameterization with the cross-term NMO velocity is generally less accurate. The selection of the set of anellipticity coefficients as the perturbation coefficients also affects the accuracy. For the parameterizations using a vertical and two horizontal velocities as the background (cases D, G, and H), the one using three cross-term anellipticity parameters (case H) is the most accurate one, whereas the parameterization specified as case G is the worst. One can say that the more cross-term anellipticity parameters we use, the more accurate result we obtain. From the overall sensitivity plots (Figures 11 and 12) and the accuracy plots (Figures 15 and 16), one can see that the less magnitude of coefficient $\hat{B}_{ij}$, the more accurate result we obtain for the traveltime approximation based on the Shanks transform. Above all, the approximation with a symmetric parameterization (case H) using a vertical and two horizontal velocities as the background model and three cross-term anellipticity parameters as the perturbation parameters results in the most accurate traveltime function.

DISCUSSIONS

In our proposed perturbation method for traveltime approximation, a different parameterization selection impacts the accuracy of the traveltime approximation due to the selection of the elliptical background and different proportion in perturbation parameters (anellipticity parameters) from the selected parameterization. This difference in traveltime error is caused by the perturbation method that is fixing the elliptical (ellipsoidal) background and fitting with the perturbation coefficients (anellipticity parameters). For the parameterization using the NMO velocities as the background model, better accuracy is obtained at a short offset. Note that we are using an offset-depth ratio of up to five (long offset) in the numerical examples, which explains the more accurate result for those using the horizontal velocities as the background. The different parameterization causes the sensitivity difference in anellipticity parameters. A more accurate result is obtained from less sensitivity in the perturbation parameters. Although the background model selection contributes most for the accuracy of the traveltime approximation using the perturbation method.

The NMO velocity might not be preserved for traveltime approximation given by the Shanks transform (equation 9) with arbitrary parameterization. Obviously, if NMO velocities are explicitly kept in the parameterization list (cases A–C), they are preserved regardless of the approximation. If NMO velocities are not in the parameterization list, they might be preserved (cases D and G) or they might not be preserved (cases E, F, and H). For example, in case H, the exact expressions for NMO velocities are

$$V_{n1} = \frac{V_{h1}}{\sqrt{(1+\eta_{xy})(1+\eta_{xz})}} \approx V_{h1}\left(1 - \frac{\eta_{xy}+\eta_{xz}}{2} + \frac{3(\eta_{xy}^2+\eta_{xz}^2)}{8} + \frac{\eta_{xy}\eta_{xz}}{4}\right),$$
$$V_{n2} = \frac{V_{h2}}{\sqrt{(1+\eta_{xy})(1+\eta_{yz})}} \approx V_{h2}\left(1 - \frac{\eta_{xy}+\eta_{yz}}{2} + \frac{3(\eta_{xy}^2+\eta_{yz}^2)}{8} + \frac{\eta_{xy}\eta_{yz}}{4}\right). \quad (14)$$

However, the Shanks transform approximation gives inaccurate NMO velocities,

$$V_{n1} = V_{h1}\sqrt{\frac{\eta_{xy}(\eta_{xz}-1)+\eta_{xz}}{\eta_{xy}+\eta_{xy}^2+\eta_{xz}+\eta_{xy}\eta_{xz}+\eta_{xz}^2}} \approx V_{h1}\left(1 - \frac{\eta_{xy}+\eta_{xz}}{2} + \frac{3(\eta_{xy}^2+\eta_{xz}^2)}{8} + \frac{\eta_{xy}\eta_{xz}}{4}\right),$$
$$V_{n2} = V_{h2}\sqrt{\frac{\eta_{xy}(\eta_{yz}-1)+\eta_{yz}}{\eta_{xy}+\eta_{xy}^2+\eta_{yz}+\eta_{xy}\eta_{yz}+\eta_{yz}^2}} \approx V_{h2}\left(1 - \frac{\eta_{xy}+\eta_{yz}}{2} + \frac{3(\eta_{xy}^2+\eta_{yz}^2)}{8} + \frac{\eta_{xy}\eta_{yz}}{4}\right). \quad (15)$$

The expressions in equations 14 and 15 are equivalent in the case of weak anellipticity.

The proposed approximation can be extended to the multilayered by using the effective model parameters from the Dix-type equations (Stovas, 2015). When there is an azimuthal variation between the multilayered ORT model, the effective parameters with different azimuthal orientation of the layers are listed in Ravve and Koren (2017) and Koren and Ravve (2017).

However, some parameterizations defined by the horizontal velocities might not be that accurate because they are in the homogeneous case because the form of the approximation is derived from the homogeneous case, whereas ray tracing for the horizontal velocities (infinite offset) is impossible for a multilayered ORT model.

CONCLUSION

We defined a group of new parameterizations by using three cross-term anellipticity parameters (η_{xy}, η_{xz}, and η_{yz}) and three cross-term NMO velocities (V_{12}, V_{13}, and V_{23}) for a homogeneous ORT model. The perturbation-based traveltime approximations are proposed in ORT media using the corresponding new parameterizations. Based on the symmetric behavior, we divide eight parameterizations into two groups and test their accuracy in traveltime in the numerical examples. The sensitivity analysis performed for perturbation coefficients at the near-, mid-, and far-offset range illustrates the different effects for a selected set of anellipticity parameters. The overall sensitivity performed for the full range of offset shows that the corresponding coefficients are proportional to the slowness squared from the given background velocity model. By comparison of eight different parameterizations, we show that the one with V_0, V_{h1}, V_{h2}, η_{xy}, η_{xz}, and η_{yz} (case H) results in the most accurate traveltime approximation based on the Shanks transform.

ACKNOWLEDGMENTS

We would like to acknowledge China Scholarship Council and the Rock Seismic (ROSE) Research Project for financial support. We also thank I. Ravve, U. Waheed, and two anonymous reviewers for their comments and helpful suggestions.

APPENDIX A

THE PERTURBATION SERIES FOR TRAVELTIME IN THE ORT MODEL USING THE PARAMETERIZATION CASE H (V_0, V_{h1}, V_{h2}, η_{xy}, η_{xz}, AND η_{yz})

The perturbation series for traveltime in ORT model is defined by (Stovas et al., 2016)

$$\tau = \tau_0 + \sum_i a_i \eta_i + \sum_{i,j} b_{ij} \eta_i \eta_j, (i,j = 1,2,3). \tag{A-1}$$

For parameterization case H with V_0, V_{h1}, V_{h2}, η_{xy}, η_{xz}, and η_{yz}, the index $1 \equiv xy$, $2 \equiv xz$, and $3 \equiv yz$ for the perturbation series in equation A-1. The elliptical background model is given by

$$\tau_0 = \sqrt{t_0^2 + \frac{x^2}{V_{h1}^2} + \frac{y^2}{V_{h2}^2}}. \tag{A-2}$$

The perturbation coefficients in equation A-1 are computed by solving the corresponding eikonal equation in equation 6 shown by

$$\begin{aligned}
a_1 &= \frac{t_0^2(\tau_{hx}^2 + \tau_{hy}^2)}{2\tau_0^3}, a_2 = \frac{\tau_{hx}^2(t_0^2 + \tau_{hy}^2)}{2\tau_0^3}, a_3 = \frac{\tau_{hy}^2(t_0^2 + \tau_{hx}^2)}{2\tau_0^3},\\
b_{11} &= -\frac{9t_0^4(\tau_{hx}^2 + \tau_{hy}^2)^2}{8\tau_0^7},\\
b_{22} &= -\frac{9\tau_{hx}^4(t_0^2 + \tau_{hy}^2)^2}{8\tau_0^7},\\
b_{33} &= -\frac{9\tau_{hy}^4(t_0^2 + \tau_{hx}^2)^2}{8\tau_0^7},\\
b_{12} &= \frac{t_0^2\tau_{hx}^2(2t_0^4 + 2\tau_{hx}^4 + \tau_{hx}^2\tau_{hy}^2 - \tau_{hy}^4 + t_0^2(-5\tau_{hx}^2 + \tau_{hy}^2))}{4\tau_0^7},\\
b_{13} &= \frac{t_0^2\tau_{hy}^2(2t_0^4 + 2\tau_{hy}^4 + \tau_{hx}^2\tau_{hy}^2 - \tau_{hx}^4 + t_0^2(-5\tau_{hy}^2 + \tau_{hx}^2))}{4\tau_0^7},\\
b_{23} &= \frac{\tau_{hx}^2\tau_{hy}^2(2\tau_{hx}^4 + 2\tau_{hy}^4 + t_0^2\tau_{hx}^2 - t_0^4 + \tau_{hy}^2(-5\tau_{hx}^2 + t_0^2))}{4\tau_0^7},
\end{aligned} \tag{A-3}$$

where $\tau_{hx} = x/V_{h1}$ and $\tau_{hy} = y/V_{h2}$.

APPENDIX B

THE PERTURBATION SERIES FOR TRAVELTIME IN THE ORT MODEL USING THE PARAMETERIZATION CASE C (V_0, V_{n1}, V_{n2}, η_{xy}, η_{xz}, AND η_{yz})

For parameterization case C with V_0, V_{n1}, V_{n2}, η_{xy}, η_{xz}, and η_{yz}, the index $1 \equiv xy$, $2 \equiv xz$, and $3 \equiv yz$ for the perturbation series in equation A-1. The elliptical background model is given by

$$\tau_0 = \sqrt{t_0^2 + \frac{x^2}{V_{n1}^2} + \frac{y^2}{V_{n2}^2}}. \tag{B-1}$$

Solving the corresponding eikonal equation with the perturbation series in equation A-1, we obtain the series coefficients a_i and b_{ij}, $(i,j = 1,2,3)$ given by

$$\begin{aligned}
a_1 &= -\frac{(\tau_{nx}^2 + \tau_{ny}^2)^2}{2\tau_0^3}, a_2 = -\frac{\tau_{nx}^4}{2\tau_0^3}, a_3 = -\frac{\tau_{ny}^4}{2\tau_0^3},\\
b_{11} &= \frac{3(\tau_{nx}^2 + \tau_{ny}^2)^3(4t_0^2 + \tau_{nx}^2 + \tau_{ny}^2)}{8\tau_0^7},\\
b_{22} &= \frac{3\tau_x^6(4t_0^2 + \tau_{nx}^2 + 4\tau_{ny}^2)}{8\tau_0^7},\\
b_{33} &= \frac{3\tau_y^6(4t_0^2 + 4\tau_{nx}^2 + \tau_{ny}^2)}{8\tau_0^7},\\
b_{12} &= \frac{\tau_{nx}^4((\tau_{nx}^2 + \tau_{ny}^2)^2 + 8t_0^2(\tau_{nx}^2 + \tau_{ny}^2) - 2t_0^4)}{4\tau_0^7},\\
b_{13} &= \frac{\tau_{ny}^4((\tau_{nx}^2 + \tau_{ny}^2)^2 + 8t_0^2(\tau_{nx}^2 + \tau_{ny}^2) - 2t_0^4)}{4\tau_0^7},\\
b_{23} &= -\frac{9\tau_{nx}^4\tau_{ny}^4}{4\tau_0^7},
\end{aligned} \tag{B-2}$$

where $\tau_{nx} = x/V_{n1}$ and $\tau_{ny} = y/V_{n2}$.

APPENDIX C

THE PERTURBATION SERIES FOR TRAVELTIME IN THE ORT MODEL USING THE PARAMETERIZATION CASE E (V_{12}, V_{13}, V_{23}, η_1, η_2, AND η_3)

For parameterization case E with V_{12}, V_{13}, V_{23}, η_1, η_2, and η_3, the elliptical background model is given by

$$\tau_0 = \sqrt{\frac{x^2}{V_{k1}^2} + \frac{y^2}{V_{k2}^2} + \frac{z^2}{V_{k0}^2}}, \tag{C-1}$$

where $V_{k0} = V_{13}V_{23}/V_{12}$, $V_{k1} = V_{12}V_{23}/V_{13}$, and $V_{k2} = V_{12}V_{13}/V_{23}$, where V_{ij} is defined in equation 4.

Solving the corresponding eikonal equation with the perturbation series in equation A-1, we obtain the series coefficients a_i and b_{ij} given by

$$a_1 = \frac{\tau_{kx}^2(-\tau_{ky}^2+\tau_{kz}^2)-\tau_{ky}^2(\tau_{ky}^2+\tau_{kz}^2)}{2\tau_0^3},$$
$$a_2 = \frac{\tau_{ky}^2(-\tau_{kx}^2+\tau_{kz}^2)-\tau_{kx}^2(\tau_{kx}^2+\tau_{kz}^2)}{2\tau_0^3},$$
$$a_3 = \frac{\tau_{kx}^2(-\tau_{kz}^2+\tau_{ky}^2)-\tau_{kz}^2(\tau_{ky}^2+\tau_{kz}^2)}{2\tau_0^3},$$
$$\begin{aligned} b_{11} = {} & \frac{1}{2\tau_0^7}(4\tau_{kx}^6\tau_{ky}^2+\tau_{kx}^4(11\tau_{ky}^4+15\tau_{ky}^2\tau_{kz}^2-9\tau_{kz}^4) \\ & +5\tau_{kx}^2\tau_{ky}^2(\tau_{ky}^2+\tau_{kz}^2)(2\tau_{ky}^2+3\tau_{kz}^2) \\ & +\tau_{ky}^2(\tau_{ky}^2+\tau_{kz}^2)^2(3\tau_{ky}^2+4\tau_{kz}^2)), \\ b_{22} = {} & \frac{1}{2\tau_0^7}(4\tau_{ky}^6\tau_{kx}^2+\tau_{ky}^4(11\tau_{kx}^4+15\tau_{kx}^2\tau_{kz}^2-9\tau_{kz}^4) \\ & +5\tau_{kx}^2\tau_{ky}^2(\tau_{kx}^2+\tau_{kz}^2)(2\tau_{kx}^2+3\tau_{kz}^2) \\ & +\tau_{kx}^2(\tau_{kx}^2+\tau_{kz}^2)^2(3\tau_{kx}^2+4\tau_{kz}^2)), \\ b_{33} = {} & \frac{1}{2\tau_0^7}(4\tau_{kx}^6\tau_{kz}^2+\tau_{kx}^4(11\tau_{kz}^4+15\tau_{ky}^2\tau_{kz}^2-9\tau_{ky}^4) \\ & +5\tau_{kx}^2\tau_{kz}^2(\tau_{ky}^2+\tau_{kz}^2)(2\tau_{kz}^2+3\tau_{ky}^2) \\ & +\tau_{kz}^2(\tau_{ky}^2+\tau_{kz}^2)^2(3\tau_{kz}^2+4\tau_{ky}^2)), \\ b_{12} = {} & \frac{1}{\tau_0^7}(\tau_{kx}^6(-\tau_{ky}^2+\tau_{kz}^2)-\tau_{kx}^4(2\tau_{ky}^4+2\tau_{ky}^2\tau_{kz}^2+\tau_{kz}^4) \\ & -\tau_{kx}^2(\tau_{ky}^6+2\tau_{ky}^4\tau_{kz}^2+15\tau_{ky}^2\tau_{kz}^4+2\tau_{kz}^6) \\ & +\tau_{ky}^2\tau_{kz}^2(\tau_{ky}^4-\tau_{ky}^2\tau_{kz}^2-2\tau_{kz}^4)), \\ b_{13} = {} & \frac{1}{\tau_0^7}(\tau_{ky}^6(-\tau_{kz}^2+\tau_{kx}^2)-\tau_{ky}^4(2\tau_{kz}^4+2\tau_{kz}^2\tau_{kx}^2+\tau_{kx}^4) \\ & -\tau_{ky}^2(\tau_{kz}^6+2\tau_{kz}^4\tau_{kx}^2+15\tau_{kz}^2\tau_{kx}^4+2\tau_{kx}^6) \\ & +\tau_{kx}^2\tau_{kz}^2(\tau_{kz}^4-\tau_{kx}^2\tau_{kz}^2-2\tau_{kx}^4)), \\ b_{23} = {} & \frac{1}{\tau_0^7}(\tau_{kz}^6(-\tau_{kx}^2+\tau_{ky}^2)-\tau_{kz}^4(2\tau_{kx}^4+2\tau_{kx}^2\tau_{ky}^2+\tau_{ky}^4) \\ & -\tau_{kz}^2(\tau_{kx}^6+2\tau_{kx}^4\tau_{ky}^2+15\tau_{kx}^2\tau_{ky}^4+2\tau_{ky}^6) \\ & +\tau_{kx}^2\tau_{ky}^2(\tau_{kx}^4-\tau_{kx}^2\tau_{ky}^2-2\tau_{ky}^4)), \end{aligned} \tag{C-2}$$

where $\tau_{kx} = x/V_{k1}$, $\tau_{ky} = y/V_{k2}$, and $\tau_{kz} = z/V_{k0}$.

APPENDIX D

THE PERTURBATION SERIES FOR TRAVELTIME IN THE ORT MODEL USING THE PARAMETERIZATION CASE F (V_{12}, V_{13}, V_{23}, η_{xy}, η_{xz}, AND η_{yz})

For parameterization case F with V_{12}, V_{13}, V_{23}, η_{xy}, η_{xz}, and η_{yz}, the index $1 \equiv xy$, $2 \equiv xz$, and $3 \equiv yz$ for the perturbation series in equation A-1. The elliptical background model is given by

$$\tau_0 = \sqrt{\frac{x^2}{V_{k1}^2}+\frac{y^2}{V_{k2}^2}+\frac{z^2}{V_{k0}^2}}, \tag{D-1}$$

where $V_{k0} = V_{13}V_{23}/V_{12}$, $V_{k1} = V_{12}V_{23}/V_{13}$, and $V_{k2} = V_{12}V_{13}/V_{23}$, where V_{ij} is defined in equation 4.

Solving the corresponding eikonal equation with the perturbation series in equation A-1, we obtain the series coefficients a_i and b_{ij} given by

$$\begin{aligned} & a_1 = -\frac{(\tau_{kx}^2+\tau_{ky}^2)^2}{2\tau_0^3}, a_2 = -\frac{(\tau_{ky}^2+\tau_{kz}^2)^2}{2\tau_0^3}, a_3 = -\frac{(\tau_{kx}^2+\tau_{kz}^2)^2}{2\tau_0^3}, \\ & b_{11} = \frac{3(\tau_{kx}^2+\tau_{ky}^2)^3(4\tau_{kz}^2+\tau_{kx}^2+\tau_{ky}^2)}{8\tau_0^7}, \\ & b_{22} = \frac{3(\tau_{ky}^2+\tau_{kz}^2)^3(\tau_{kz}^2+4\tau_{kx}^2+\tau_{ky}^2)}{8\tau_0^7}, \\ & b_{33} = \frac{3(\tau_{kx}^2+\tau_{kz}^2)^3(\tau_{kz}^2+\tau_{kx}^2+4\tau_{ky}^2)}{8\tau_0^7}, \\ & b_{12} = \frac{\tau_{kx}^4(\tau_{ky}^4-6\tau_{ky}^2\tau_{kz}^2-9\tau_{kz}^4)+\tau_{kx}^2(2\tau_{ky}^6-4\tau_{ky}^4\tau_{kz}^2-6\tau_{ky}^2\tau_{kz}^4)+\tau_{ky}^4(\tau_{ky}^2+\tau_{kz}^2)^2}{4\tau_0^7}, \\ & b_{13} = \frac{\tau_{ky}^4(\tau_{kx}^4-6\tau_{kx}^2\tau_{kz}^2-9\tau_{kz}^4)+\tau_{ky}^2(2\tau_{kx}^6-4\tau_{kx}^4\tau_{kz}^2-6\tau_{kx}^2\tau_{kz}^4)+\tau_{kx}^4(\tau_{kx}^2+\tau_{kz}^2)^2}{4\tau_0^7}, \\ & b_{23} = \frac{\tau_{kx}^4(\tau_{kz}^4-6\tau_{ky}^2\tau_{kz}^2-9\tau_{ky}^4)+\tau_{kx}^2(2\tau_{kz}^6-4\tau_{ky}^4\tau_{kz}^2-6\tau_{ky}^2\tau_{kz}^4)+\tau_{kz}^4(\tau_{ky}^2+\tau_{kz}^2)^2}{4\tau_0^7}, \end{aligned} \tag{D-2}$$

where $\tau_{kx} = x/V_{k1}$, $\tau_{ky} = y/V_{k2}$, and $\tau_{kz} = z/V_{k0}$.

REFERENCES

Alkhalifah, T., 2003, An acoustic wave equation for orthorhombic anisotropy: Geophysics, **68**, 1169–1172, doi: 10.1190/1.1598109.

Alkhalifah, T., 2011, Scanning anisotropy parameters in complex media: Geophysics, **76**, no. 2, U13–U22, doi: 10.1190/1.3553015.

Alkhalifah, T., 2013, Traveltime approximations for inhomogeneous transversely isotropic media with a horizontal symmetry axis: Geophysical Prospecting, **61**, 495–503, doi: 10.1111/j.1365-2478.2012.01067.x.

Alkhalifah, T., and R.-É. Plessix, 2014, A recipe for practical full-waveform inversion in anisotropic media: An analytical parameter resolution study: Geophysics, **79**, no. 3, R91–R101, doi: 10.1190/geo2013-0366.1.

Alkhalifah, T., and I. Tsvankin, 1995, Velocity analysis for transversely isotropic media: Geophysics, **60**, 1550–1566, doi: 10.1190/1.1443888.

Bender, C. M., and S. A. Orszag, 1978, Advanced mathematical methods for scientists and engineers: McGraw-Hill.

Červený, V., 2001, Seismic ray theory: Cambridge University Press.

Fomel, S., 2004, On anelliptic approximations for qP velocities in VTI media: Geophysical Prospecting, **52**, 247–259, doi: 10.1111/j.1365-2478.2004.00413.x.

Fomel, S., and A. Stovas, 2010, Generalized nonhyperbolic moveout approximation: Geophysics, **75**, no. 2, U9–U18, doi: 10.1190/1.3334323.

Fowler, P. J., 2003, Practical VTI approximations: A systematic anatomy: Journal of Applied Geophysics, **54**, 347–367, doi: 10.1016/j.jappgeo.2002.12.002.

Gholami, Y., R. Brossier, S. Operto, A. Ribodetti, and J. Virieux, 2013, Which parameterization is suitable for acoustic vertical transverse isotropic full waveform inversion? Part 1: Sensitivity and trade-off analysis: Geophysics, **78**, no. 2, R81–R105, doi: 10.1190/geo2012-0204.1.

Golikov, P., and A. Stovas, 2012, Accuracy comparison of nonhyperbolic moveout approximations for qP-waves in VTI media: Journal of Geophysics and Engineering, **9**, 428–432, doi: 10.1088/1742-2132/9/4/428.

Grechka, V., and I. Tsvankin, 1999a, 3-D moveout velocity analysis and parameter estimation for orthorhombic media: Geophysics, **64**, 820–837, doi: 10.1190/1.1444593.

Grechka, V., and I. Tsvankin, 1999b, 3-D moveout inversion in azimuthally anisotropic media with lateral velocity variation: Theory and a case study: Geophysics, **64**, 1202–1218, doi: 10.1190/1.1444627.

Koren, Z., and I. Ravve, 2017, Fourth-order normal moveout velocity in elastic layered orthorhombic media — Part 2: Offset-azimuth domain: Geophysics, **82**, no. 3, C113–C132, doi: 10.1190/geo2016-0222.1.

Masmoudi, N., and T. Alkhalifah, 2014, Multi-parameters scanning in HTI media: 84th Annual International Meeting, SEG, Expanded Abstracts, 480–485.

Masmoudi, N., and T. Alkhalifah, 2016, Traveltime approximations and parameter estimation for orthorhombic media: Geophysics, **81**, no. 4, C127–C137, doi: 10.1190/geo2015-0367.1.

Ravve, I., and Z. Koren, 2017, Fourth-order normal moveout velocity in elastic layered orthorhombic media — Part 1: Slowness-azimuth domain: Geophysics, **82**, no. 3, C91–C111, doi: 10.1190/geo2015-0621.1.

Schoenberg, M., and K. Helbig, 1997, Orthorhombic media: Modeling elastic wave behavior in a vertically fractured earth: Geophysics, **62**, 1954–1974, doi: 10.1190/1.1444297.

Sripanich, Y., and S. Fomel, 2015, On anelliptic approximations for qP velocities in transversely isotropic and orthorhombic media: Geophysics, **80**, no. 5, C89–C105, doi: 10.1190/geo2014-0534.1.

Stovas, A., 2015, Azimuthally dependent kinematic properties of orthorhombic media: Geophysics, **80**, no. 6, C107–C122, doi: 10.1190/geo2015-0288.1.

Stovas, A., N. Masmoudi, and T. Alkhalifah, 2016, Application of perturbation theory for P-wave eikonal equation in orthorhombic media: Geophysics, **81**, no. 6, C309–C317, doi: 10.1190/geo2016-0097.1.

Tsvankin, I., 1997, Anisotropic parameters and P-wave velocity for orthorhombic media: Geophysics, **62**, 1292–1309, doi: 10.1190/1.1444231.

Tsvankin, I., 2005, Seismic signatures and analysis of reflection data in anisotropic media, 2nd ed.: SEG.

Tsvankin, I., 2012, Seismic signatures and analysis of reflection data in anisotropic media: SEG, Geophysical References Series 19.

Vasconcelos, I., and I. Tsvankin, 2006, Non-hyperbolic moveout inversion of wide-azimuth P-wave data for orthorhombic media: Geophysical Prospecting, **54**, 535–552, doi: 10.1111/j.1365-2478.2006.00559.x.

Xu, S., A. Stovas, and Q. Hao, 2017, Perturbation-based moveout approximations in anisotropic media: Geophysical Prospecting, **65**, 1218–1230.

Yilmaz, O., 2001, Seismic data analysis: Processing, inversion, and interpretation of seismic data: Investigations in geophysics: SEG.